

# Reanalysis of the OGLE-I Observations with the Image Subtraction Method I. Galactic bar fields MM1-A, MM1-B, MM7-A, and MM7-B<sup>1</sup>

by

A. Pigulski, Z. Kołaczkowski and G. Kopacki

Wrocław University Observatory, Kopernika 11, 51-622 Wrocław, Poland  
E-mails: (pigulski, kolaczk, kopacki)@astro.uni.wroc.pl

*Received ...*

## ABSTRACT

As a result of the reanalysis of the OGLE-I observations by means of the image subtraction method, we present the first part of a catalog, consisting of the data for variable stars in four Galactic fields observed by the OGLE-I, viz. MM1-A, MM1-B, MM7-A, and MM7-B. In total, 2016 variable stars have been found. This increased the number of known variable in these fields stars more than twofold. We comment on the detectability of the variable stars in previous studies.

Some interesting findings are also discussed. Among others, we found 45  $\delta$  Scuti stars (38 are new) including several multiperiodic objects. Detailed analysis of the light curves of 47 RR Lyrae stars (24 are new detections) allowed us to find five stars which exhibit nonradial pulsations and one RRd star. Three RRab stars are members of the Sagittarius dwarf galaxy (Sgr dSph). We also find four objects which are probably galactic RV Tauri stars and one W Virginis star which seems to belong to Sgr dSph. This is the first Population II Cepheid found in this satellite galaxy and dSph other than the Fornax one.

For eclipsing EW-type binaries, which are the most abundant variables in our catalog, we investigate the amplitude and period distributions. A comparison with the previous OGLE-I catalogs indicates that we found more stars with smaller amplitudes. Finally, in addition to the two microlensing events discovered previously in these fields, we find five more.

**Keywords:** *Stars: Variables – Stars:  $\delta$  Scuti – Stars: RR Lyrae – Catalogs*

## 1. Introduction

Thousands of variable stars have been discovered in the central regions of our Galaxy by the Optical Gravitational Lensing Experiment (OGLE), a long-term microlensing project which in June 2001 entered its third stage of operation, OGLE-III<sup>2</sup>. In the first part of the project (OGLE-I; Udalski *et al.* 1992), observations were collected in four seasons (1992–1995) with the 1-m Swope telescope of the Las Campanas Observatory. Twenty  $15' \times 15'$  fields (see below) have been monitored frequently enough to allow reliable time-series analysis.

During the second part of the OGLE project (OGLE-II; Udalski *et al.* 1997b), carried out in the years 1997–2000, observations were obtained with a dedicated 1.3-m Warsaw Telescope at the same observatory. A new,  $2K \times 2K$  CCD detector was used in a drift-scan mode, resulting in a  $2K \times 8K$  frame covering a field of view of  $14' \times 57'$ .

Almost all Galactic fields observed by the OGLE are very rich in stars. The profile-fitting photometry in such fields is severely affected by crowding. This reduces detectability of variable stars. Fortunately, a new method of finding variable stars in crowded fields, based on image subtraction, has been developed when the OGLE-II project was in operation (Alard and Lupton 1998; Alard 2000). Since the method proved to be very efficient in the detection of variable stars in crowded fields, it was implemented by Woźniak (2000) in his

<sup>1</sup>Based on observations obtained in the Las Campanas Observatory of the Carnegie Institution of Washington.

<sup>2</sup>See <http://www.astrouw.edu.pl/~ogle/>

Difference Image Analysis (DIA) package and then applied to the OGLE-II observations of 49 Galactic fields. This analysis resulted in a catalog consisting of  $\sim 200,000$  candidates for variables in the central regions of the Galaxy (Woźniak *et al.* 2002).

The methods, direct profile fitting and image subtraction, are complementary and, when used together, provide complete information on the incidence of the variability in the observed fields.

Although most OGLE-I fields have been covered by the OGLE-II and are observed within the OGLE-III projects carried out with better detectors, there are still several reasons why the reanalysis of the OGLE-I observations with the image subtraction can yield valuable results. Firstly, in view of the completeness the method provides, its application would certainly yield new variable stars. Next, for those stars which were already discovered, the DIA would provide better photometry. From the point of view of a study of the long-term behavior of variable stars, it is a very good reason. Finally, a comparison of the detectability by the image subtraction and profile-fitting methods is possible.

The OGLE-I data cover twenty fields (BWC, BW1 to BW11, MM1-A, MM1-B, MM3, MM5-A, MM5-B, MM7-A, MM7-B, and GB1) with a number of frames suitable for time-series analysis. Except for the fields BW9–BW11, GB1, MM1-A/B and MM3 which were not observed in 1992, observations in four seasons, 1992–1995, are available.

In this series of papers we plan to provide a complete information on the variability of stars in these twenty OGLE-I fields, based on the results of reanalysis of the OGLE-I observations by means of the DIA. We will include also the less numerous (20–50 per field)  $V$ -filter observations, reported for variable stars by Szymański *et al.* (2001) only. In the present paper, the first of the series, we report the results of the search in four fields, MM1-A, MM1-B, MM7-A, and MM7-B, located in the Galactic bar, a few degrees north-east of the Baade’s Window (BW). The second paper will include fields MM3, MM5-A, MM5-B and GB1, while the third one, all twelve BW fields. Since the adjacent OGLE-I fields slightly overlap, we shall report the observations of a given variable star including data from all overlapping fields.

The variables discovered earlier in the OGLE-I data are briefly summarized in the next section. The method we use to search for variable stars is outlined in Sect. 3, whereas the fourth section describes the entries of the catalog we provide. Section 5 includes the comparison of the detectability of variable stars. Finally, comments on different types of variable stars are given in Sect. 6.

## 2. Known Variables

As far as the catalogs of variable stars are concerned, so-far published results from the OGLE-I data are the following. The most important one is the Catalog of Periodic Variable Stars (CPVS) containing 2861 periodic variables with the mean  $I_C$  magnitude brighter than 18 mag. The catalog has been published for sixteen of the twenty fields mentioned above in five papers (Udalski *et al.* 1994; 1995a,b; 1996; 1997a). A similar catalog was not published for four fields, MM1-A, MM1-B, GB1, and MM3. Additions to the CPVS include a list of 116 long-period and non-periodic variable stars published by Żebruń (1998, hereafter Z98), 11 variables discovered in the vicinity of 20 microlensing events found in the OGLE-I data (Woźniak and Szymański 1998, hereafter WS98), and recently published catalog of 2084 periodic variables (Szymański *et al.* 2001; hereafter SKU01), mainly fainter than  $I_C \approx 18$  mag. Variable stars in the latter paper were divided into two categories: contact binaries and pulsating variable stars.

The known variable stars discovered in the four OGLE-I fields under consideration (MM1-A, MM1-B, MM7-A, MM7-B) are summarized in Table 1. For the OGLE-I microlensing events (MLE), their numbers from WS98 (preceded by “#”) are given. Other variables found by WS98 are labeled as VAR. SKU01 discoveries are reported separately for their contact binaries (EW) and pulsating stars (P). Figure 1 shows the equatorial co-

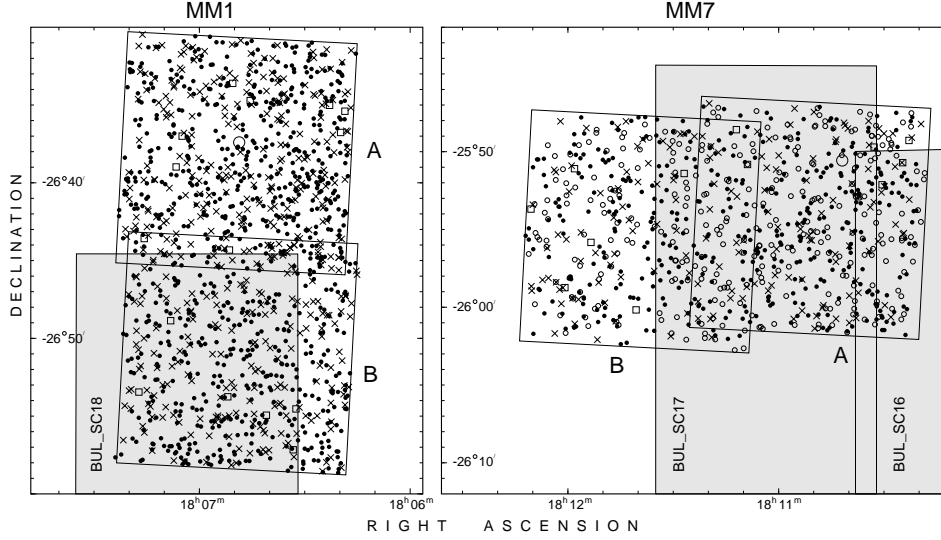


Figure 1: Location of variable stars in fields MM1 and MM7. The symbols have the following meaning: circles, stars in the CPVS (U97); crosses, stars found by SKU01; squares, long-period variables discovered by Z98 and WS98, large circles, the OGLE-I microlensing events, OGLE#9 in field MM7-A and OGLE#14 in field MM1-A. The new variable stars we found are shown as small dots. The grey areas indicate the OGLE-II fields (labeled).

ordinates of variable stars. As we mentioned earlier, CPVS includes variable stars for the fields MM7-A and MM7-B (Udalski *et al.* 1997a, hereafter U97), but not for MM1.

Table 1  
Variables discovered by U97, Z98, WS98 and SKU01 in four analyzed OGLE-I fields: MM1-A, MM1-B, MM7-A, and MM7-B.

OGLE-I field	Number of variables (only new)				Total
	U97	Z98	WS98 (VAR + MLE)	SKU01 (EW + P)	
MM1-A	—	9	0 + 1 (#14)	156 + 78	244
MM1-B	—	5	1 + 0	131 + 55	192
MM7-A	182	4	0 + 1 (#9)	72 + 15	274
MM7-B	112	7	0 + 0	48 + 24	191
Total	294	25	1 + 2	407 + 172	901

It has to be noted that rectangle areas around MM1 and MM7 OGLE-I fields shown in Fig. 1 contain no objects listed in the General Catalog of Variable Stars (GCVS, Kholopov *et al.* 1988), the Name Lists 67–76 which followed that catalog (see Kazarovets *et al.* 2001), and the New Catalogue of Suspected Variable Stars (Kukarkin *et al.* 1982) with the Supplement (Kazarovets *et al.* 1998).

The MM1 fields have been partly covered by OGLE-II field BUL\_SC18 and MACHO field 101, whereas the MM7 fields were covered by OGLE-II fields BUL\_SC16 and BUL\_SC17 and MACHO field 178 (see Fig. 1).

The third part of the All Sky Automated Survey (ASAS-3, Pojmański 2002) will also cover this area, but the catalog of variables from this part of the sky has not been published yet. It will, however, contain variable stars which are brighter than the saturation limit for stars in the OGLE-I data ( $I_C \approx 14$  mag).

### 3. The Method

The calibrated OGLE-I observations used in our analysis have been kindly made accessible to us by Prof. Andrzej Udalski. They were obtained through two filters, matching Gunn  $i$  and Johnson  $V$  bands (the former is easily transferable to Cousins  $I_C$ , see Udalski *et al.* 1992). Most observations were carried out with the Gunn  $i$  filter. Before starting reductions we excluded some frames polluted by scattered light and those with short exposure times. The number of frames used in the final calculations is given in Table 2. In this table, we specify the frames which were used to calculate the reference image. The frames used as reference ones in astrometric interpolations are shown with boldface in the fifth column.

Using the information provided with the frames, we have chosen frames with the smallest seeing and low background to calculate the reference image needed for image subtraction (See Table 2). Typically, 6–7 frames in the Gunn  $i$  filter and 3–4 frames in the Johnson  $V$  filter were used for this purpose.

T a b l e 2  
Data for the OGLE-I fields studied in this paper

OGLE-I field	Coordinates (field center)		Filter	Number of frames	Frames used to create a reference image
	$\alpha_{2000}$	$\delta_{2000}$			
MM1-A	18 <sup>h</sup> 06 <sup>m</sup> 49.5 <sup>s</sup>	−26°37′59″	$V$	23	10295, 10609, 11470
			$i$	143	10053, 10108, <b>10460</b> , 10610, 10865, 11469, 11779
MM1-B	18 <sup>h</sup> 06 <sup>m</sup> 49.7 <sup>s</sup>	−26°50′57″	$V$	22	10210, 10297, 11471
			$i$	132	10054, <b>10109</b> , 10250, 10822, 10866, 11290, 11468
MM7-A	18 <sup>h</sup> 10 <sup>m</sup> 53.2 <sup>s</sup>	−25°54′15″	$V$	26	11263, 11606, 12016, 12211
			$i$	168	10204, 10443, <b>10547</b> , 11456, 11590, 11734
MM7-B	18 <sup>h</sup> 11 <sup>m</sup> 39.8 <sup>s</sup>	−25°55′05″	$V$	26	11264, 11303, 12017, 12212
			$i$	171	10101, 10158, <b>10444</b> , 10548, 11455, 11637, 11735

The procedure of the image subtraction has been explained in detail in the original papers (Alard and Lupton 1998, Alard 2000, Woźniak 2000) and will not be repeated here. We only mention that the image subtraction algorithm requires a reference image which is subsequently convolved with a kernel in order to match seeing in a given image and then subtracted from it. As a result, difference image is obtained. The difference images can be stacked to form a “variability map” which is used for detecting variables. The reference image and the variability map for a given field (and filter) were obtained by means of the DIA package of Woźniak (2000). The  $2K \times 2K$  images were divided into  $8 \times 8 = 64$  square sub-fields which have been processed independently. However, the variable search procedure implemented in the DIA turned out not to detect many apparent variable stars in the variability map. We therefore replaced it by the Daophot (Stetson 1987) FIND routine run on the variability map. The output was a list of candidates for variable stars which has been sent back to the DIA which calculated light curve for each candidate.

In an ideal case, all stars appearing in the variability map should be variable. For several reasons this was not the case. For the OGLE-I data, a huge number of spurious candidates for variables has been produced by the chip defects. Typically, about 20,000 variable candidates per field have been obtained. Only 2–3% of them appeared to be true variables. In order to extract them in an automatic way, we calculated the AoV periodogram of Schwarzenberg-Czerny (1996) in the range between 0 and  $30 \text{ d}^{-1}$  for each candidate. In order to increase the detection efficiency, the light curves have been first cleaned for

outliers (we used  $5\sigma$  clipping) and observations with large errors (they were not rejected from further analysis, however). The AoV periodogram provides the parameter  $\theta$  which has been used as a threshold. It has to be noted that this procedure allows also detection of non-periodic variables since such variables yield high peaks in the vicinity of 0 and  $1 \text{ d}^{-1}$ .

After this step, we were usually left with 700–1000 candidates for variables in a field. A light curve of each of these stars was checked visually, period(s) refined, and the classifications made. The script we used created a single plot showing: (i) flux difference as a function of time, (ii) phase diagram (the correct period could be selected from the list of highest peaks in periodogram, allowing also its doubling, a common case for eclipsing binaries), (iii) a part of the periodogram in the vicinity of the strongest peak, (iv) a part of the reference image and variability map with the analyzed star centered. At this stage, observations in both filters were used.

#### 4. The Catalog

In total, we found 2016 variable stars in the four OGLE-I fields analyzed in this paper (see Table 3). As we shall discuss in Sect. 5, we have recovered 84% of variable stars discovered by previous investigators and, in addition, found 1255 new variables. This means that we increased the number of variables in fields MM1 and MM7 more than twofold.

Table 3  
The number of variables discovered in fields MM1 and MM7 according to class. The thirteen classes of variables are defined in Sect. 4.2.

Field	Type of variability												Total	
	DSCT	RRc	RRab	CEP	Mira	EW	EB	EA	SIN	NSIN	PER	APER		MLE
Known														
MM1	2	5	—	—	—	289	18	12	—	—	15	4	1	346
MM7	5	5	13	1	—	220	20	62	6	7	68	8	—	415
Both	7	10	13	1	—	509	38	74	6	7	83	12	1	761
New														
MM1	26	6	17	4	9	229	23	122	45	29	290	43	3	846
MM7	12	—	1	—	2	151	6	39	31	25	119	21	2	409
Both	38	6	18	4	11	380	29	161	76	54	409	64	5	1255
All														
MM1	28	11	17	4	9	518	41	134	45	29	305	47	4	1192
MM7	17	5	14	1	2	371	26	101	37	32	187	29	2	824
Both	45	16	31	5	11	889	67	235	82	61	492	76	6	2016

The two MM1 fields, MM1-A and MM1-B, slightly overlap (Fig. 1). The same is true for the two MM7 fields. This means that some variables can be found in both fields. We therefore report the variables using designations which indicate only a combined field, MM1 or MM7.

The parameters of all variable stars we found are given in Tables 4a (field MM1) and 4b (field MM7), available in the full form in the *Acta Astronomica Archive* (see cover page) and our WWW page

<http://www.astro.uni.wroc.pl/ldb/ogle1/>

Here, only a sample page of Table 4b is shown. The tables include: star name, its equatorial coordinates, classification (see Sect. 4.2), period(s), reference magnitude and color, number of data points and cross-identifications with previous OGLE catalogs. If no cross-identification is given, the variable is a new one.

We also present our results in a graphical form. A sample plot is displayed in Fig. 2. The plots showing light curves and finding charts can be found on our WWW page as gzipped PostScript files. The following file names have been used:  $\langle field \rangle \langle variability class \rangle \langle sequential number \rangle .ps$ ; for example file “MM1\_EW\_2.ps” includes the second

page with the light curves and finding charts for EW-type eclipsing binaries in the field MM1. If there was only one page for a given class, no sequential number was given.

T a b l e 4b  
Variable stars in field MM7. The full table is available in an electronic form only. Here, the entries for the first 50 stars are shown as an example.

Var. name	$\alpha_{2000.0}$	$\delta_{2000.0}$	Var. type	Period [d]	$N_I$	$N_V$	$I_C$	$(V - I_C)$	Cross-identifications
MM7-0001	18 10 34.39	-25 48 28.5	DSCT	0.04604239	165	25	15.526	0.969	
MM7-0002	18 10 26.50	-25 48 36.8	DSCT	0.04959108	157	0	17.718	1.563	
MM7-0003	18 11 47.40	-25 48 08.8	DSCT	0.05584052	164	19	16.026	1.383	
				0.05701629					
				0.0636008					
MM7-0004	18 11 04.87	-25 56 47.6	DSCT	0.06580976	162	26	14.979	0.793	
MM7-0005	18 11 55.37	-25 55 19.5	DSCT HADS	0.06583299	167	23	17.445	1.417	OGLE MM7-B V87 (DSCT)
MM7-0006	18 10 20.77	-25 52 07.8	DSCT	0.06674510	165	26	16.985	1.161	
				0.0686684					
MM7-0007	18 10 22.39	-25 48 02.6	DSCT	0.06808241	159	25	16.331	1.176	
MM7-0008	18 12 02.43	-25 53 32.2	DSCT	0.0732052	160	22	15.761	1.190	
MM7-0009	18 10 28.65	-25 49 11.3	DSCT HADS	0.07884756	166	25	17.242	1.143	OGLE MM7-A V103 (DSCT)
MM7-0010	18 10 41.83	-25 54 56.0	DSCT	0.08860681	165	26	16.813	1.150	
				0.0904652					
MM7-0011	18 10 49.84	-25 56 47.4	DSCT	0.0934265	160	26	15.616	1.097	
MM7-0012	18 11 08.12	-26 00 56.3	DSCT	0.09588007	166	25	16.379	1.224	
				0.1247319					
				0.0766860					
MM7-0013	18 10 48.67	-25 52 58.5	DSCT HADS	0.15885904	150	21	16.932	1.396	OGLE MM7-A V88 (DSCT)
MM7-0014	18 12 06.28	-25 52 13.1	DSCT	0.1677467	169	23	17.135	1.793	
MM7-0015	18 10 32.14	-25 59 55.7	DSCT	0.1723239	159	26	15.465	2.060	
MM7-0016	18 10 22.80	-25 53 04.7	DSCT HADS/EW	0.1972421	162	0	18.882	—	SKU MM7A.19894 (EWs)
MM7-0017	18 10 26.01	-25 58 54.7	DSCT/EW	0.2066995	155	25	17.433	1.757	OGLE MM7-A V139 (EW) = = SKU MM7A.4811 (EWs)
MM7-0018	18 10 54.50	-25 49 42.4	RRc	0.22759215	147	26	15.942	1.125	OGLE MM7-A V44 (RRc)
MM7-0019	18 10 49.72	-25 48 24.0	RRc	0.2749935	161	26	17.048	1.568	OGLE MM7-A V94 (RRc)
MM7-0020	18 11 33.45	-25 55 08.3	RRc	0.2867497	157	21	15.802	1.330	OGLE MM7-B V14 (RRc)
MM7-0021	18 10 35.61	-25 52 51.8	RRc	0.2878246	156	26	16.180	1.534	OGLE MM7-A V47 (RRc)
MM7-0022	18 10 39.85	-25 59 15.0	RRc NR	0.3066806	168	26	16.030	1.251	SKU MM7A.34501 (EWa, P = 0.64918 d)
				0.3245838					
MM7-0023	18 10 48.96	-25 56 29.8	RRab	0.4436107	146	26	16.349	1.175	OGLE MM7-A V26 (RRab)
MM7-0024	18 10 32.07	-25 59 36.2	RRab	0.4938028	168	26	15.619	1.741	OGLE MM7-A V25 (RRab)
MM7-0025	18 11 18.64	-26 00 41.3	RRab	0.52984105	330	48	16.068	1.449	OGLE MM7-A V20 (RRab)
MM7-0026	18 11 12.65	-25 49 37.5	RRab	0.5304776	318	49	15.969	1.593	OGLE MM7-A V34 (RRab)
MM7-0027	18 11 40.09	-25 51 02.8	RRab	0.5332197	164	23	15.860	1.319	OGLE MM7-B V13 (RRab)
MM7-0028	18 12 03.44	-25 58 22.2	RRab	0.5391315	165	23	15.569	1.492	OGLE MM7-B V6 (RRab)
MM7-0029	18 11 00.07	-25 57 38.0	RRab	0.5408001	155	26	15.025	1.534	OGLE MM7-A V2 (RRab)
MM7-0030	18 11 30.96	-25 56 01.8	RRab	0.5538256	170	23	16.350	1.263	
MM7-0031	18 12 00.30	-25 53 19.9	RRab	0.5593891	153	22	15.629	1.423	OGLE MM7-B V8 (RRab)
MM7-0032	18 11 14.73	-25 51 46.6	RRab	0.5670927	162	23	15.847	1.295	OGLE MM7-A V16 (RRab)
MM7-0033	18 11 51.14	-25 58 11.8	RRab	0.590028	167	23	15.793	1.209	OGLE MM7-B V7 (RRab)
MM7-0034	18 11 44.86	-25 58 03.1	RRab	0.616314	165	0	18.545	2.197	SKU MM7B.75698 (P)
MM7-0035	18 11 47.90	-25 52 23.2	RRab	0.6180556	160	23	17.369	1.649	OGLE MM7-B V63 (RRab)
MM7-0036	18 11 36.71	-25 49 06.7	RRab	0.8812044	167	23	15.607	1.622	OGLE MM7-B V12 (RRab)
MM7-0037	18 11 12.01	-25 55 51.1	EW	0.23476895	320	48	18.086	1.859	SKU MM7A.168828 (EWs)
MM7-0038	18 11 05.38	-25 55 03.1	EW	0.2634260	157	25	14.841	1.673	
MM7-0039	18 11 25.78	-26 00 21.4	EW	0.2637791	96	0	—	—	
MM7-0040	18 11 50.72	-25 52 39.1	EW	0.2670858	167	23	18.591	2.089	SKU MM7B.108382 (EWa)
MM7-0041	18 10 43.62	-26 00 44.2	EW	0.2690071	160	0	—	—	SKU MM7A.65167 (EWa)
MM7-0042	18 10 54.51	-25 49 11.2	EW	0.2722634	162	0	—	—	
MM7-0043	18 11 22.51	-25 53 10.7	EW	0.2779473	138	0	17.318	1.749	
MM7-0044	18 10 49.20	-25 51 12.7	EW	0.2788253	155	0	18.230	—	
MM7-0045	18 11 35.76	-25 58 39.6	EW	0.2794520	167	0	18.183	2.087	
MM7-0046	18 10 54.08	-25 54 38.3	EW	0.2842176	163	24	18.689	1.613	SKU MM7A.109242 (P)
MM7-0047	18 11 35.90	-25 54 59.1	EW	0.2877905	159	22	17.576	1.783	
MM7-0048	18 11 09.85	-25 55 39.6	EW	0.2884005	326	49	17.538	1.652	OGLE MM7-A V138 (EW) = SKU MM7A.168261 (EWa)
MM7-0049	18 11 51.36	-26 00 56.4	EW	0.2931527	157	0	19.493	2.063	
MM7-0050	18 10 58.47	-25 51 26.3	EW	0.2932039	154	0	19.623	—	

Typically, three panels for a given star are presented in a plot (see Fig. 2). For periodic stars and stars with a dominating period shorter than 25 days the left-hand panel shows the light curve as a phase diagram. For periodic stars with dominating period longer than 25 days and stars classified as APER, MLE and MIRA the light curve is presented as a function of heliocentric Julian day (this is not shown in Fig. 2). The star name (Sect. 4.1), period (P) or dominating period (D) as well as cross-identifications are also plotted in this panel. The right-hand top panel shows a finding chart of  $99 \times 99$  pixels ( $43'' \times 43''$ ) from the frame used as a reference one and oriented roughly in such a way that north is up, east to the left. The variable star is centered and encircled with a light-grey circle. Some additional informations on the star (classification, coordinates, magnitudes) are given in the right-hand bottom panel.

For some stars, more than one plot is presented. This has been done for short-period multiperiodic stars, when in addition to a phase diagram showing original data folded with the main period, we also show all detected periodicities separately (that is, folded after

removing the other ones, see Fig. 2 for MM7-0022). In a few cases, when a strong trend was apparent, we removed it and show the phase diagram once again, but freed from the trend. In such cases plots contain a remark “trend removed”. When the data from two overlapping fields are combined, an encircled letter “C” is plotted right of our star name (see plots for MM7-0025 and MM7-0037 in Fig. 2).

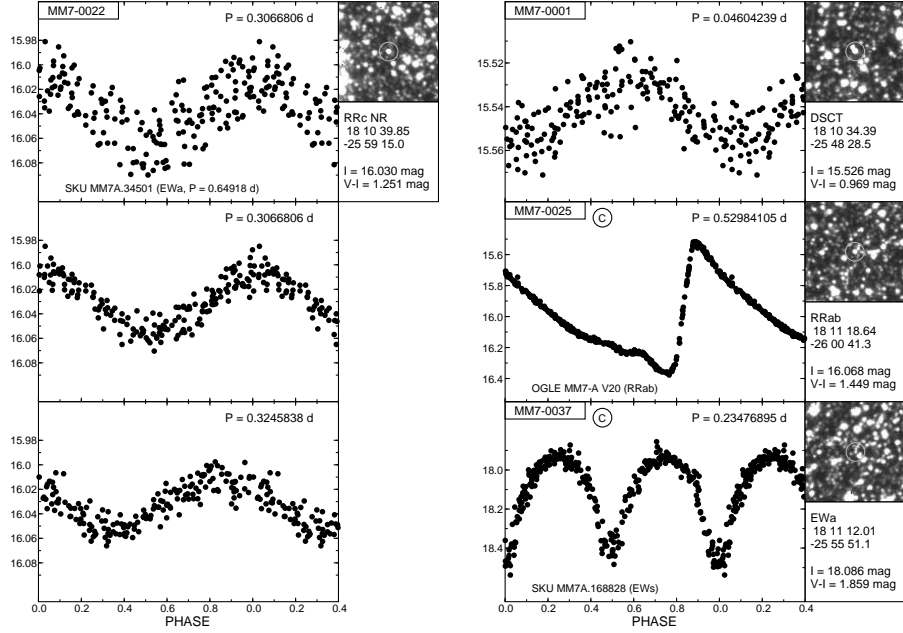


Figure 2: A sample page of the graphical data which include  $I_C$ -filter light curves and finding charts for variables in our catalog. Typically, data for 20 or 30 stars are plotted in a single page. Here, for clarity, we show only the data for four selected stars in the field MM7. The ordinate is the  $I_C$ -filter magnitude; phase 0.0 was chosen arbitrarily. See text for more explanations.

There were some variable stars which were too faint or too crowded to be detected by Daophot in the reference image. In such cases, a correct transformation from fluxes to magnitudes (see Sect. 4.4) could not be performed. For these stars we do not give the mean magnitudes and/or colors in plots and tables. However, in order to show the light curves of all stars on the magnitude scale, we assumed that the magnitudes of these stars are close to the limiting magnitude in the reference frame and did the transformation. This helps to estimate the amplitude, but it must be remembered that the magnitudes of these stars could be unreliable.

#### 4.1. Designation of variables

The already known variables from the OGLE catalogs will be referred to using designations introduced by their authors. The CPVS introduced the names of variable stars consisting of a field designation, letter “V” and a sequential number. In this catalog (see, e.g., U97) the stars were arranged according to the decreasing mean brightness. The microlensing events were numbered separately (OGLE #1 to OGLE #20; WS98). Z98 introduced new designations for his long-period variables (e.g., OGLE-LT-V011). On the other hand, SKU01 and WS98 use for their variables the numbers from the OGLE photometric database. We shall refer to these variables using the following abbreviations: SKU for SKU01 and WS for WS98, original field name and star number, e.g., SKU MM1B.24085. The OGLE catalogs provide the coordinates and finding charts, so that the proper identifi-

cation or cross-identification is rather easy.

The extensions of some of the above-mentioned numbering systems could be somewhat misleading. Therefore, we decided to introduce our own designations consisting of the field name (without division into part A or B, if two adjacent fields were observed) and a four-digit number, e.g., MM1-0019. The stars in Tables 4a and 4b and in the plots described above are presented in groups, according to the classification scheme explained in the next subsection. Within a given group, the stars are arranged according to the increasing period (or dominating period), except for aperiodic stars and microlensing events which are presented in the order of increasing right ascension.

#### 4.2. The classification scheme

Many variable stars reported in this paper are periodic or multiperiodic. In the process of classification of these stars we have taken into account the following features: period(s), amplitude, the shape of the light curve, and—in some cases—the location in the color-magnitude diagram. As far as the stars with periods below  $\sim 1$  d are concerned, the classification was quite easy and rather unambiguous. Among stars with longer periods, only the Miras are easily recognizable.

The following types of variability have been attributed to the periodic pulsating stars:

- DSCT –  $\delta$  Scuti stars. If the light curve had the  $I_C$ -filter full amplitude larger than 0.1 mag, the designation HADS (high-amplitude  $\delta$  Scuti star) was given in addition to DSCT. Note that some of the HADS, especially with the shortest periods, can be Population II pulsators, known as SX Phoenicis stars.
- RRc – RR Lyrae stars of Bailey type c. We also included one RRd star (double-mode RR Lyrae star) into this group. For RRc stars with nonradial modes present, the “NR” designation has been added (this applies also to RRab stars).
- RRab – RR Lyrae stars of Bailey type ab.
- CEP – Cepheid variables and RV Tauri stars.
- MIRA – Miras.

Classifying eclipsing binaries we have adopted an old system based on the morphology of the light curve which divides these stars into three categories. These are: W Ursae Majoris-type (EW),  $\beta$  Lyrae-type (EB), and Algol-type (EA). However, the distinction between EB and EA or EB and EW depends on the quality of the light curve. Consequently, the classification of the eclipsing binaries is somewhat arbitrary for some stars. If a distinct O’Connell effect was observed, the designation “OC” was added.

The presence of large scatter causes that two stars with light curves of exactly the same shape can be classified in a different way. There is, however, no way to avoid this problem. Hence, for some stars double classification is given (e.g. EW/DSCT) in the order of the authors’ preference.

The classification of stars that show periodicities longer than  $\sim 1$  d is more difficult. Most of these stars were classified as miscellaneous (MISC) in the CPVS. Some are strictly periodic, but there are too many possible types of variability in a given range of periods to make a correct classification. If the light curve is non-sinusoidal or there is an evidence of multiperiodicity, a final decision can be sometimes made. Such is the case of some ellipsoidal variables. We finally decided to divide the stars into the three following categories:

- SIN – Stars with sinusoidal light curves showing the evidence of a single periodicity. This category may include such variables as the monoperoiodic Slowly Pulsating B-type (SPB) stars,  $\alpha^2$  Canum Venaticorum stars,  $\gamma$  Doradus stars, also some ellipsoidal variables (with half the orbital period) and chromospherically active stars, etc.

- NSIN – Stars with strictly periodic light curves, which are evidently non-sinusoidal. The ellipsoidal variables (“ELL” designation added) can present such light curves, but other types of variability are also possible in this group.
- PER – Stars with a dominating periodicity, but showing also amplitude and/or phase changes or the periodic changes superimposed on the variability on a longer time-scale. A majority of semi-regular variables fall into this category.

In addition, stars showing aperiodic behaviour were classified as:

- APER – Stars that show aperiodic light variations. It has to be noted that stars with linear light changes that might arise from high proper motion (see Eyer and Woźniak 2001, Soszyński *et al.* 2002), but also from the intrinsic light variation, were not included in our catalog.
- MLE – Microlensing events.

#### 4.3. Multiperiodicity

The correct period (or periods) of a light variation was decided during the classification process and was found by means of the AoV periodogram using solely the  $I_C$ -filter data. The final period reported in Tables 4a and 4b represents, however, a refined value obtained from a nonlinear least-squares solution. The least-squares fit was done also for non-sinusoidal light curves; in such a case the appropriate number of harmonics was fitted to the data. Depending on the accuracy of the period determination, periods are given with a different number of digits.

The search for multiperiodicity was made only for some groups of stars, namely DSCT, RRC, RRab, CEP and some SIN and PER stars with the shortest periods. This reflects the scientific interests of the authors. The results are discussed in Sect. 6. Thus, it is still possible that some stars we do not announce to be multiperiodic, especially from the SIN and PER groups have, in fact, multiple periods.

#### 4.4. Conversion from the fluxes to magnitudes

The DIA provides differential fluxes in arbitrary units. In order to convert the fluxes into magnitudes we first derived the instrumental magnitudes of all stars in the reference frame by means of a standard profile-fitting photometry, namely using Daophot package of Stetson (1987). This was done for each of the four fields (MM1-A, MM1-B, MM7-A, MM7-B) and the two filters (Johnson  $V$ , Gunn  $i$ ) separately. The instrumental magnitudes,  $p = \{v, i\}$ , were used to derive the coefficients of the transformation equation:

$$P_k = -2.5 \log(f_0 + f_k) + C, \quad (1)$$

where  $f_0 = 10^{-0.4(p+C_2)}$  was the reference flux expressed in the same units as the differential fluxes,  $f_k$ , for the  $k$ th measurement.  $P_k$  stands for the corresponding  $k$ th measurement taken from the  $P = \{V, I_C\}$  photometry of U97 and SKU01. Using stars in common with U97 and/or SKU01, we first derived the values of  $f_0$  and  $C$  for each star. It appeared that  $C$  varies slightly with the instrumental magnitude,  $p$ . Therefore, we adopted a linear form of the dependence,  $C = a + b \cdot (p - 15.0)$ , and derived the coefficients  $a$  and  $b$  by means of the least squares. Then, with  $C(p)$  fixed, the  $f_0$  values were recalculated and finally, the constant  $C_2$  was determined. The final coefficients are given in Table 5. There are many possible sources of the weak dependence of  $C$  on  $p$ , including small nonlinearities of the detector indicated by Udalski *et al.* (1992). We shall not speculate on that. Taking into account the small color terms in the transformation to the standard  $V I_C$  system (Udalski *et al.* 1992), our transformation should give reliable standard magnitudes as well.

Table 5

The coefficients of the transformation from differential fluxes to the standard  $VI_C$  magnitudes for fields MM1 and MM7.

Field	Filter	$a$ [mag]	$b$	$C_2$ [mag]	RSD [mag]
MM1A	$V$	$25.7827 \pm 0.0188$	$0.0395 \pm 0.0136$	$-22.8063 \pm 0.0167$	0.096
	$I_C$	$25.0856 \pm 0.0087$	$0.0238 \pm 0.0094$	$-22.7038 \pm 0.0148$	0.074
MM1B	$V$	$25.7786 \pm 0.0361$	$0.0668 \pm 0.0218$	$-22.8267 \pm 0.0170$	0.130
	$I_C$	$25.0458 \pm 0.0103$	$0.0225 \pm 0.0098$	$-22.7954 \pm 0.0159$	0.079
MM7A	$V$	$25.4173 \pm 0.0154$	$0.0465 \pm 0.0124$	$-22.7987 \pm 0.0193$	0.025
	$I_C$	$25.0083 \pm 0.0066$	$0.0392 \pm 0.0075$	$-22.7745 \pm 0.0068$	0.072
MM7B	$V$	$25.5806 \pm 0.0274$	$0.0646 \pm 0.0217$	$-22.6753 \pm 0.0240$	0.062
	$I_C$	$25.0345 \pm 0.0054$	$0.0145 \pm 0.0059$	$-22.7809 \pm 0.0081$	0.048

Having derived the coefficients  $a$ ,  $b$ , and  $C_2$  for each field/filter combination we could transform the differential fluxes for all variable stars into the standard  $VI_C$  magnitudes. However, since the instrumental magnitudes were derived by means of the profile-fitting photometry in a crowded field from a *single* reference frame, the errors of the transformation could be quite large. Thus, the magnitudes should be used with caution. The photometry (both the differential fluxes and the transformed magnitudes) is available on the web page given above.

The reference magnitudes of variable stars were also transformed to the standard  $VI_C$  magnitudes. They are given in Tables 4a and 4b and in our plots (see Fig. 2). Very few variable stars were not found in the reference frame. In these cases we assumed they have the instrumental magnitude close to the limiting magnitude of the photometry in a given reference frame. For these stars the reference magnitudes and/or colors were not included in Tables 4a and 4b. We used them only for plotting a star's light curve, so that in our plots all stars would have the ordinate given in magnitudes.

#### 4.5. Equatorial coordinates

Equatorial coordinates of variable stars were derived using their positions in the variability map. For each field we identified about 4000 stars from the Hubble *Guide Star Catalog*, ver. 2.2.1, and used a third-order polynomial to transform each coordinate into an appropriate equatorial one. The accuracy of the final position depends primarily on the accuracy of the position in the variability map; we estimate it to be of the order of  $0.2''$ . There are systematic differences up to  $1''$  between our coordinates and those given in OGLE catalogs. They occur probably because of using different astrometric catalogs as a reference.

## 5. Comments on Detectability

It is interesting to check how many variable stars presented in the OGLE catalogs mentioned in Sect. 2 could be recovered by means of the DIA. Out of the 294 variables from the CPVS, detected in the two MM7 fields (Table 1), we have recovered 284, that is about 97%. The fact that the remaining 10 stars were not detected can be explained as follows:

- (i) The DIA provides no photometry for stars which are overexposed in the reference frame. This is the reason why the two brightest stars in the CPVS, MM7-A V1 and MM7-B V1, were missed.
- (ii) Since some areas around overexposed pixels are marked as unusable, stars which fall there will have no DIA photometry either. This was the case for MM7-A V112 and MM7-B V100.

- (iii) There are some shifts between the frames. The DIA software detects only these variables which are located in the region common with the reference frame. Three CPVS stars, MM7-A V8, V56 and V114, were outside this region.
- (iv) If the star has a low amplitude and/or is faint, it may be too faint in the variability map to be detected by the search procedure. This was the case MM7-A V172.
- (v) This rather rare case happens when Daophot search procedure cannot resolve variables which are very close to each other. This was the case for MM7-A V133 which is very close to MM7-A V77. In consequence, the former star was not detected.

In addition, we found one CPVS star (MM7-A V86) which can be barely seen in the variability map but was detected. However, after careful analysis we concluded that it shows no clear evidence for variability. We therefore regard it as constant so it does not appear in our catalog.

Z98 reports 26 variable stars in fields MM1 and MM7 (Table 1). One, OGLE-LT-V106, is identical with MM7-A V116, so that 25 stars are new detections. We recover them all but OGLE-LT-V108 because of point (ii). In addition, two other stars, OGLE-LT-V001 and OGLE-LT-V024, are probably not real variables, but rather high-proper motion stars, showing nearly linear change of brightness if constant position is used to get the magnitudes (Eyer and Woźniak 2001; Soszyński *et al.* 2002). We do not include them either.

We also detect a variable found by WS98 in field MM1-B (WS MM1B.198992). Of the two microlensing events, OGLE#9 in field MM7-A and OGLE#14 in MM1-A, we detect only the latter. The former was too faint in the variability map to be detected (see point (iv) above).

SKU01 report 591 new variable stars in fields MM1 and MM7, but some have double designations, so that there are actually 579 (407 classified as eclipsing, EW, and 172 as pulsating, P; see Table 1) new variables. We recovered 100 out of 120 EW stars (83%) and 20 out of 39 P stars (51%) in the field MM7. In fields MM1 the detection efficiencies are slightly higher. This is because the CPVS did not include this field, so the bright variable stars located there were discovered by SKU01. We found 250 out of 287 EW stars (87%) and 83 out of 133 P stars (62%) in field MM1. The main reason for non-detections is point (iv) above: stars are too faint in the variability map to be detected. Some other stars are not detected because they are very close to overexposed stars (point (ii)).

While the small difference between the detection efficiency in fields MM1 (79%) and MM7 (75%) is understandable in view of the comments given above, the large difference in the detectability of the EW (86%) and P stars (60%) is rather a surprise. Both classes have similar distribution in brightness, so that the brightness difference is not the explanation. Moreover, out of 103 P stars we recovered in this study, only eight (8%) were classified as pulsating stars in our catalog, RRc or DSCT. Remaining P variables are almost exclusively EW-type eclipsing binaries. Recalling the fact that among variables classified by SKU01 as EW we found four pulsating stars, we conclude that the algorithm used by SKU01 to distinguish eclipsing and pulsating stars by means of the Fourier coefficients apparently did not work well. The stars classified as P have probably lower amplitudes than the EW stars, as can be seen from Fig. 14 of SKU01. This explains both the large spread of Fourier coefficients in the decomposition shown by SKU01 (their Fig. 1) and much lower detection efficiency of P stars in comparison with EW stars in our catalog.

## 6. Comments on Individual Variable Stars

A thorough analysis of the contents of the presented catalog is out of scope of this paper. However, taking into account our personal interests, we shall discuss in detail the results for some of the variables we found.

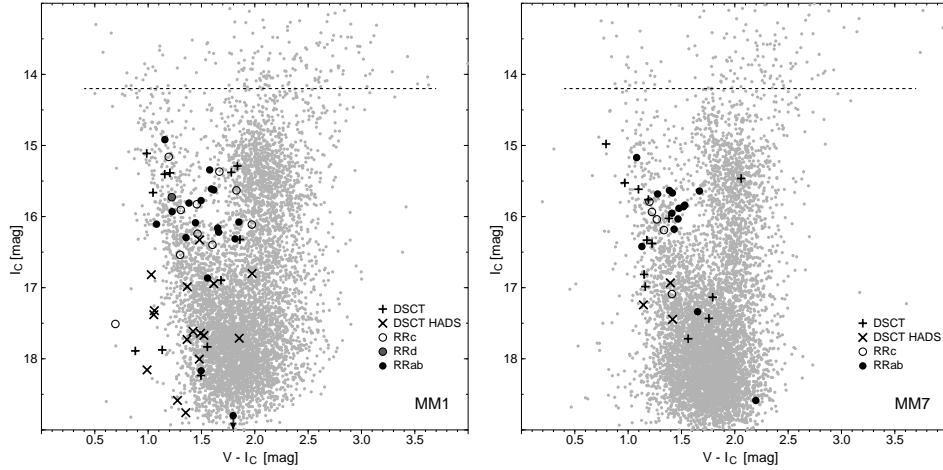


Figure 3: Color-magnitude diagrams for field MM1 (left) and MM7 (right). Only about 10% of stars with the best photometry ( $\sigma_{V-I} < 0.1$  mag) is shown (as grey dots). Positions of  $\delta$  Scuti and RR Lyrae stars are plotted with different symbols. The saturation limit is shown as a dashed line.

### 6.1. $\delta$ Scuti stars

Some  $\delta$  Scuti stars were included in the CPVS, but because this search was limited to frequencies up to only  $10 \text{ d}^{-1}$  and stars brighter than  $I_C \approx 18$  mag, it is clear that mainly High-Amplitude  $\delta$  Scuti (HADS) stars had been detected and that many low-amplitude  $\delta$  Scuti stars could be still found. This is indeed the case: we found 45  $\delta$  Scuti stars, of which only 7 were known from U97 and SKU01. Seven stars show clearly multiperiodic behaviour; as many as three significant periodicities were found in MM7-0003 and MM7-0012. Fifteen stars in field MM1 and four stars in MM7 could be classified as the HADS. The location of  $\delta$  Scuti stars in the colour-magnitude diagram (CMD) is shown in Fig. 3. While the low-amplitude variables are mostly disk stars, the HADS, lying 1 to 3 mag below RR Lyraes, seem to be mainly at the bulge distance. The same was found by Alcock *et al.* (2000a) from their analysis of a much larger sample of the bulge HADS. If they are normal, evolved main-sequence HADS, this would be an indication of the presence of a not so old (age  $< 1.5\text{--}2$  Gyr) stellar population at those distances. However, it is more likely they are SX Phoenicis stars of the old disk/bulge population or a mixture of both.

### 6.2. RR Lyrae stars

These stars have large amplitudes. Therefore, we expected that, at least in fields MM7, no new variables would be detected. It appeared, however, that even in these fields we were able to find a new RRab star, MM7-0030. It avoided earlier detection because of its location close to several bright stars. Out of the remaining 5 RRc and 13 RRab stars in fields MM7, CPVS reported sixteen and SKU01 added two. One of the latter, MM7-0022 = SKU MM7A.34501, is a very interesting example of an RRc star showing two close modes with periods of  $P_1 = 0.3066806$  d and  $P_2 = 0.3245838$  d and almost equal amplitudes in  $I_C$  (see the left side of Fig. 2). It was classified by SKU01 as an EWs variable (EW-type eclipsing binary with similar depth of both eclipses) and period equal to  $2P_2$ .

In fields MM1 we found 28 RR Lyrae variables. Only five of them (all of type RRc) were reported by SKU01. This is because SKU01 focused on the short-period EW-type binaries and not only RRab, but also other variables with longer periods were not presented there (see Table 3). The sample of RR Lyrae variables in field MM1 includes 11 RRc and 17 RRab stars. Among them there are five stars showing multiperiodic behaviour. The periods of all multiperiodic RR Lyrae stars we found are listed in Table 5. This table is

therefore supplementary to the recent work of Moskalik and Poretti (2003). These authors analyzed the whole CPVS sample of 215 RR Lyrae stars finding 38 multiperiodic stars, including a double-mode RRd star, BW7 V30. We also find one RRd star, MM1-0033, with the radial first-overtone to fundamental period ratio equal to  $0.737571 \pm 0.000005$ .

Another very interesting RR Lyrae star is MM1-0046, an RRab type star showing three close equally spaced frequencies, characteristic for the Blazhko effect. In this respect the star is very similar to the star BW6 V20 analyzed in detail by Moskalik and Poretti (2003).

T a b l e 5

Multiperiodic RR Lyrae variables in fields MM1 and MM7. In parentheses, the r.m.s. errors of the last two digits of preceding numbers are given.

Name in the catalog	Type <sup>a</sup>	Primary period $P_0 = f_0^{-1}$ [d]	Secondary period $P_1 = f_1^{-1}$ [d]	Frequency difference $\Delta f = f_1 - f_0$ [d <sup>-1</sup> ]
MM1-0033	RRd	0.3049400(08)	0.413438(07)	-0.860593(16)
MM1-0034	RR1- $\nu$ 1	0.3063829(05)	0.306245(04)	+0.001470(14)
MM1-0044	RR0- $\nu$ 1	0.5179836(15)	0.521618(14)	-0.013451(26)
MM1-0046	RR0-BL	0.5336114(12)	0.536120(07)	-0.008769(13)
			0.531090(08)	+0.008897(16)
MM1-0051	RR0- $\nu$ 1	0.5816272(14)	0.579520(21)	+0.006249(36)
MM7-0022	RR1- $\nu$ 1	0.3066806(14)	0.3245838(16)	-0.179853(7)

<sup>a</sup> According to Alcock *et al.*'s (2000c) classification scheme.

The position of the RR Lyrae variables in the CMD is shown in Fig. 3. A majority of them is located at the bulge distance as indicated by previous investigators (Udalski 1998, Alcock *et al.* 1998, Morgan *et al.* 1998), but three (MM1-0047, MM1-0054, MM7-0034) that are  $\sim 2$  mag fainter than the rest, are members of the Sagittarius dwarf galaxy (Sgr dSph, Mateo *et al.* 1995; Alard 1996; Alcock *et al.* 1997, 1998). The other three RR Lyrae stars lie in between, they have  $17.0 < I_C < 17.5$  mag. These are MM1-0031 = SKU MM1A.5623, MM7-0019 = OGLE MM7-A V94 and MM7-0035 = OGLE MM7-B V63. The latter was indicated as a member of Sgr dSph by Olech (1997). However, their membership is rather doubtful and a larger interstellar extinction could also explain their position in the CMD.

### 6.3. Eclipsing binaries

Eclipsing binaries constitute about 60% of stars in our catalog, of them the EW-type stars are most common. This enables us to make some statistical considerations related to this type of stars. The properties of the OGLE-I EW-type binaries have been already studied by Ruciński (1995, 1997a,b, 1998a,b) using a sample of CPVS EW-type systems from nine BW fields. He found that these stars are almost evenly distributed along the line of sight and only very few had estimated distances comparable to that of the Galactic bulge. This conclusion is in good agreement with position of these stars in the CMD (Fig. 4), where they populate the left branch consisting of the main-sequence stars and stars close to the turn-off point at different distances. Several EW stars lie close to the red clump because of blending with red stars.

Many other interesting results have been given in the above-mentioned papers of Ruciński with a clear indication that EW-type binaries can play an important role in the study of stellar populations towards and even in the bulge. In his studies, the period and amplitude distributions were used frequently to constrain properties of EW-type stars. It is, therefore, interesting to compare how the newer discoveries in the OGLE-I fields, namely those of SKU01 and the one reported in this paper, affect these two distributions. Although in this study we do not analyze BW fields, but fields in the Galactic bar, it was shown by SKU01 (their Fig. 9) that at least the period distribution of EW stars for the bar fields (MM1, MM3, MM5 and MM7) does not differ significantly from that in the BW fields.

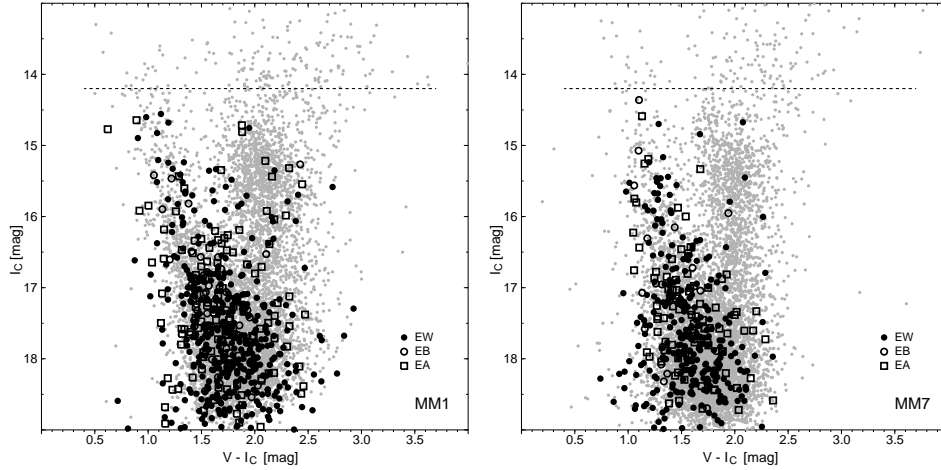


Figure 4: The same as in Fig. 3, but with positions of eclipsing binaries (EW, EB, EA) indicated.

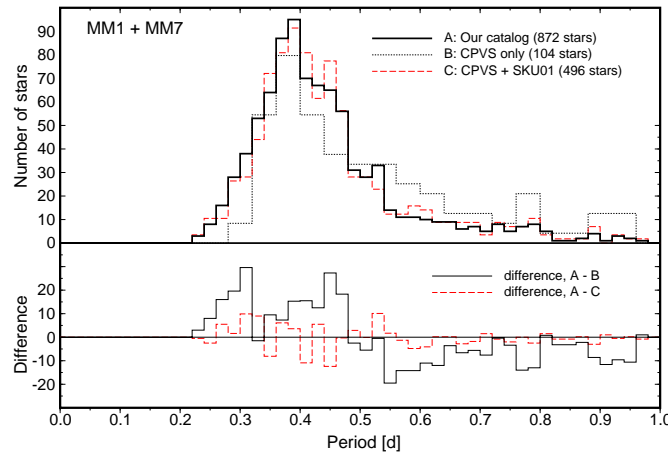


Figure 5: A comparison of period distributions for EW-type binaries with  $P < 1$  d in fields MM1 and MM7. Three distributions are shown in the top panel: for 104 CPVS stars we found in MM7-A/B (B, dotted line), for all known stars from CPVS and SKU01 we recovered (C, dashed line) and finally, for all EW stars in our catalog (A, thick solid line). All distributions were normalized to the same number of stars. In the lower panel, the differences between the distributions are shown.

A comparison of the period distributions is shown in Fig. 5. The distribution calculated for EW stars with periods shorter than 1 d from our catalog (solid line, 872 stars) was compared with two others: that consisting of the CPVS EW stars from fields MM7 only (104 stars) and all 496 already known stars (CPVS + SKU01). All distributions were normalized to the same number of stars. As can be seen from the figure, there is no significant difference between the distribution for our and SKU01 EW binaries. On the other hand, in comparison with CPVS we have an excess of stars with  $P < 0.5$  d (and consequently a deficit of stars with  $P > 0.5$  d). Two conclusions can be drawn from these differences: (i) in comparison with profile-fitting photometry, the DIA provides better completeness, but does not reach fainter stars, (ii) the difference in limiting magnitudes of the CPVS and SKU01/our catalog resulted in different period distributions. The latter can be understood in view of the period-luminosity relation for the EW stars: at a given distance, a contact binary with shorter orbital period consists of smaller (and cooler) components and thus is

fainter.

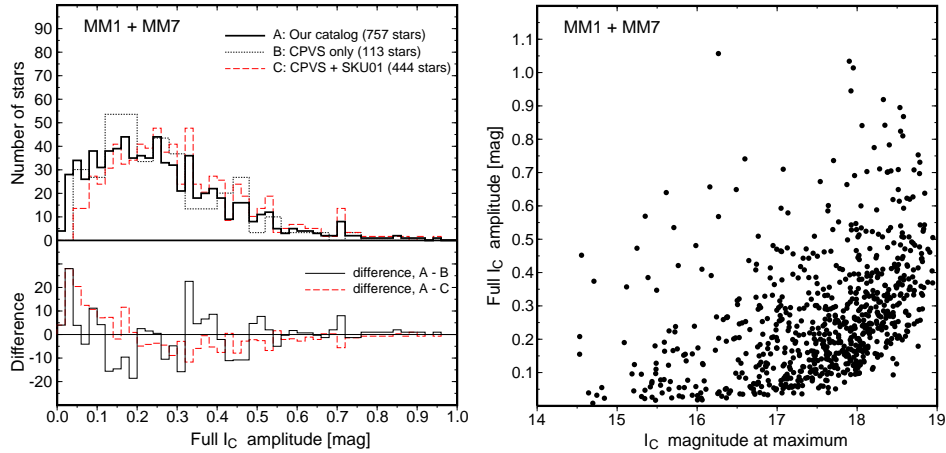


Figure 6: Left: A comparison of  $I_C$  amplitude distributions for EW-type binaries with  $I_C < 19$  mag. See Fig. 5 for the explanation of the data sets. All distributions were normalized to the same number of stars. Right: Full  $I_C$ -filter amplitudes plotted as a function of the  $I_C$  magnitude at the phase of maximum light.

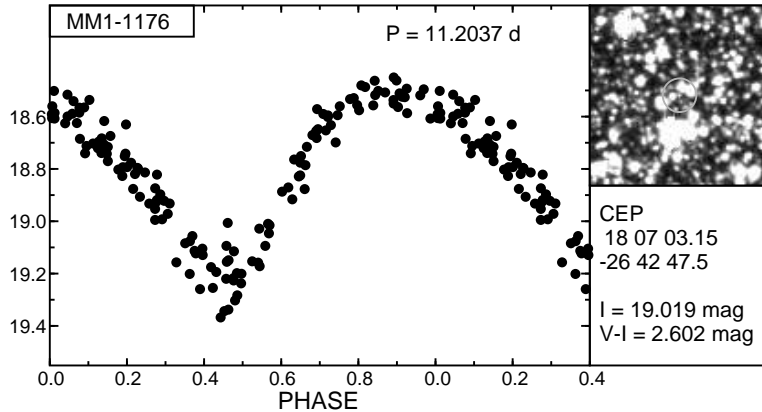


Figure 7: The  $I_C$ -filter light curve of MM1-1176, the first W Virginis star which is a likely member of the Sgr dSph.

We also compared the amplitude distributions (Fig. 6). The analyzed samples of stars are slightly different, because now we used all EW stars with  $I_C < 19$  mag at the phase of maximum light. In addition, we excluded all variable stars that were not detected in the reference frame. As can be seen from Fig. 6, we found relatively more low-amplitude stars than did SKU01, although—as expected—many faint EW stars with small amplitudes are not detected (see the right panel of Fig. 6).

#### 6.4. Cepheids, RV Tauri Stars and Miras

Classical Cepheids trace relatively young population, so they are not expected to be present in the Galactic bulge. Moreover, owing to their high luminosities, they should be overexposed in the OGLE-I observations even at the bulge distance. However, some Population II Cepheids and RV Tauri stars could be present and detected. The latter stars are not always easily recognized from long-period Population II Cepheids and are closely related to them (Wallerstein 2002), so we discuss them jointly.

There are four stars in our catalog which were classified as RV Tauri stars (we use designation CEP for them as explained in Sect. 4.2). All show alternating deeper and shallower minima in the light curve, characteristic for this group (see, e.g., Pollard *et al.* 1996). Their (doubled) periods range from about 23 days for MM7-0820 to 105 d for MM1-1179. The fifth star which was included in the CEP group, MM1-1176, is the most interesting. According to its period equal to 11.2 d, large amplitude and an asymmetric light curve (see Fig. 7), it could be Population II Cepheid of W Virginis type. However, it is very faint and red;  $I_C \approx 19.0$  mag,  $(V - I_C) \approx 2.6$  mag. Assuming it has an intrinsic color  $(V - I_C)_0 \approx 0.5$  mag and adopting  $A_{I_C} = 1.57E(V - I_C)$  (Dean *et al.* 1978) we get  $I_{C,0} \approx 15.7$  mag. Giving the mean distance modulus of Sgr dSph of 17–17.5 mag and its extended structure, MM1-1176 could be indeed a W Virginis-type star, the first known in this galaxy. So far, Population II Cepheids were found only in one of the nine Milky Way dwarf spheroidal galaxies, namely the Fornax one (Bersier and Wood 2002). Since Population II Cepheids are in a very short AGB or post-AGB evolutionary phase, they can be found only in populous dwarf galaxies. Fornax and Sagittarius dSphs are the two most luminous galaxies of this type among the Milky Way Galaxy satellites (van den Bergh 2000).

We find also 11 Miras, all are new variable stars. They were, however, detected mainly at the phase close to the minimum light.

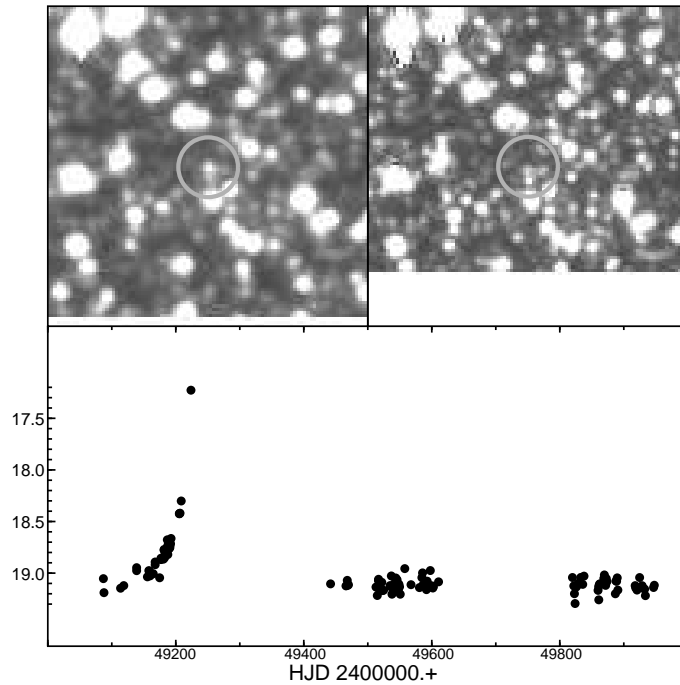


Figure 8: The  $I_C$  light-curve of the microlensing event MM1-1189. The top left panel shows a part of the mr5262 frame made on August 24, 1993 (the epoch of the brightest point in the light curve). The top right panel shows the same area in the reference image which was combined from the frames taken in 1995, about 2 years after the event.

### 6.5. Microlensing events

Six stars showing a single event of brightness increase were found. We cannot exclude the possibility that they are eruptive stars, but the most plausible explanation is that they all are microlensing events. Only one of them, OGLE #14, was known earlier (see WS98). As an example, we show in Fig. 8 the light curve of MM1-1189, and also two maps of the region, a reference frame made of the frames well outside the epoch of the event and the

frame when the star was brightest. The star is practically not visible in the reference frame, being blended with another faint star. It is, however, clearly seen in the other frame despite much poorer seeing.

It is difficult to say how many new microlensing events will be found in the remaining 16 OGLE-I fields, but because there were only two known in fields MM1 and MM7, we expect at least to double their number in the OGLE-I data. The full analysis of these events will be carried out as soon as all the OGLE-I fields are catalogued. It is interesting to note that the application of image subtraction led to doubling the number of detected microlensing events also in OGLE-II (Udalski *et al.* 2000, Woźniak *et al.* 2001) and MACHO (Alcock *et al.* 2000b) data.

### 6.6. Other stars

The largest number of new discoveries came for stars we classified as SIN, NSIN, PER, and APER — 85% of them are new variables. As can be seen in Fig. 9, they populate mostly the red branch of the CMD. However, some are relatively blue. It is therefore possible that some SIN or PER stars with periods shorter than 4 d, shown as circles in Fig. 9, are slowly pulsating B-type (SPB) stars.

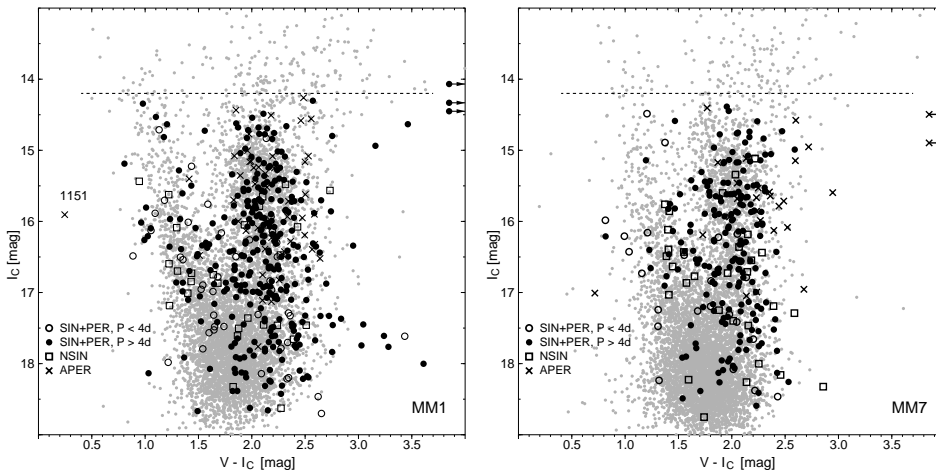


Figure 9: The same as in Fig. 3, but with SIN, NSIN, PER, and APER stars plotted. The leftmost cross in the left panel, labeled “1151”, denotes the position of the R Coronae Borealis variable MM1-1151 = OGLE-LT-V035 (Z98).

There are two interesting stars among those classified as APER. The first one is MM1-1151 = OGLE-LT-V035 classified by Żebruń (1998) as an R Coronae Borealis-type variable. It is also the bluest variable star we found (Fig. 9). The other, MM7-0813, shows several eruptions during the time covered by observations. It is identical with OGLE II BUL\_SC17\_4122, classified recently as a dwarf nova by Cieslinski *et al.* (2003).

### Acknowledgements

It is a great pleasure to express our appreciation to the whole OGLE team for their superb work and especially for their policy to present the data as soon as possible to the astronomical community. In particular, we thank Prof. A. Udalski for making available the original OGLE-I observations of the Galactic fields. We also thank Dr. P. Woźniak for allowing us to use his DIA package and K. Żebruń and I. Soszyński for explaining its details. The comments of Prof. M. Jerzykiewicz were very helpful for improving the paper.

This work was supported by the KBN grant 2 P03D 006 19.

## REFERENCES:

- Alard, C. 1996, *Astrophys. J.*, **458**, L17.
- Alard, C. 2000, *Astron. Astrophys. Suppl.*, **144**, 363.
- Alard, C., and Lupton, R.H. 1998, *Astrophys. J.*, **503**, 325.
- Alcock, C. *et al.* 1997, *Astrophys. J.*, **474**, 217.
- Alcock, C. *et al.* 1998, *Astrophys. J.*, **492**, 190.
- Alcock, C. *et al.* 2000a, *Astrophys. J.*, **536**, 798.
- Alcock, C. *et al.* 2000b, *Astrophys. J.*, **541**, 734.
- Alcock, C. *et al.* 2000c, *Astrophys. J.*, **542**, 257.
- Bersier, D., and Wood, P.R. 2002, *Astron. J.*, **123**, 840.
- Cieslinski, D., Diaz, M.P., Mennickent, R.E., and Pietrzyński, G. 2003, *Publ. Astron. Soc. Pacific*, **115**, 193.
- Dean, J.F., Warren, P.R., and Cousins, A.W.J. 1978, *Monthly Not. Royal Astron. Soc.*, **183**, 569.
- Eyer, L., and Woźniak, P.R. 2001, *Monthly Not. Royal Astron. Soc.*, **327**, 601.
- Kazarovets, E.V., Samus, N.N., and Durlevich, O.V. 1998, *Inf. Bull. Var. Stars* **4655**.
- Kazarovets, E.V., Samus, N.N., and Durlevich, O.V. 2001, *Inf. Bull. Var. Stars* **5135**.
- Kholopov, P.N. *et al.* 1988, *General Catalog of Variable Stars*, ed. 4, Moscow: Nauka Publishing House.
- Kukarkin, B.V. *et al.* 1982, *New Catalogue of Suspected Variable Stars*, Moscow: Nauka Publishing House.
- Mateo, M., Kubiak, M., Szymański, M., Kałużny, J., Krzemiński, W., and Udalski, A. 1995, *Astron. J.*, **110**, 1141.
- Morgan, S.M., Simet, M., and Bargaquast, S. 1998, *Acta Astron.*, **48**, 341.
- Moskalik, P., and Poretti, E. 2003, *Astron. Astrophys.*, **398**, 213.
- Olech, A. 1997, *Acta Astron.*, **47**, 183.
- Pojmański, G. 2002, *Acta Astron.*, **52**, 397.
- Pollard, K.R., Cottrell, P.L., Kilmartin, P.M., and Gilmore, A.C. 1996, *Monthly Not. Royal Astron. Soc.*, **279**, 949.
- Ruciński, S.M. 1995, *Astrophys. J.*, **446**, L19.
- Ruciński, S.M. 1997a, *Astron. J.*, **113**, 407.
- Ruciński, S.M. 1997b, *Astron. J.*, **113**, 1112.
- Ruciński, S.M. 1998a, *Astron. J.*, **115**, 1135.
- Ruciński, S.M. 1998b, *Astron. J.*, **116**, 2998.
- Schwarzenberg-Czerny, A. 1996, *Astrophys. J.*, **460**, L107.
- Soszyński, I. *et al.* 2002, *Acta Astron.*, **52**, 143.
- Stetson, P.B. 1987, *Publ. Astron. Soc. Pacific*, **99**, 191.
- Szymański, M., Kubiak, M., and Udalski, A. 2001, *Acta Astron.*, **51**, 259 (SKU01).
- Udalski, A. 1998, *Acta Astron.*, **48**, 113.
- Udalski, A., Szymański, M., Kałużny, J., Kubiak, M., and Mateo, M. 1992, *Acta Astron.*, **42**, 253.
- Udalski, A., Kubiak, M., Szymański, M., Kałużny, J., Mateo, M., and Krzemiński, W. 1994, *Acta Astron.*, **44**, 317.
- Udalski, A., Szymański, M., Kałużny, J., Kubiak, M., Mateo, M., and Krzemiński, W. 1995a, *Acta Astron.*, **45**, 1.
- Udalski, A., Olech, A., Szymański, M., Kałużny, J., Kubiak, M., Mateo, M., and Krzemiński, W. 1995b, *Acta Astron.*, **45**, 433.
- Udalski, A., Olech, A., Szymański, M., Kałużny, J., Kubiak, M., Mateo, M., Krzemiński, W., and Stanek, K.Z. 1996, *Acta Astron.*, **46**, 51.
- Udalski, A., Olech, A., Szymański, M., Kałużny, J., Kubiak, M., Mateo, M., Krzemiński, W., and Stanek, K.Z. 1997a, *Acta Astron.*, **47**, 1 (U97).
- Udalski, A., Kubiak, M., and Szymański, M. 1997b, *Acta Astron.*, **47**, 319.
- Udalski, A., Żebruń, K., Szymański, M., Kubiak, M., Pietrzyński, G., Soszyński, I., and Woźniak, P.R. 2000, *Acta Astron.*, **50**, 1.
- van den Bergh, S. 2000, *Publ. Astron. Soc. Pacific*, **112**, 529.
- Wallerstein, G. 2002, *Publ. Astron. Soc. Pacific*, **114**, 689.
- Woźniak, P.R. 2000, *Acta Astron.*, **50**, 451.
- Woźniak, P.R., and Szymański, M. 1998, *Acta Astron.*, **48**, 269 (WS98).
- Woźniak, P.R., Udalski, A., Szymański, M., Kubiak, M., Pietrzyński, G., Soszyński, I., and Żebruń, K. 2001, *Acta Astron.*, **51**, 175.

Woźniak, P.R., Udalski, A., Szymański, M., Kubiak, M., Pietrzyński, G., Soszyński, I., and Żebruń, K. 2002, *Acta Astron.*, **52**, 129.  
Żebruń, K. 1998, *Acta Astron.*, **48**, 289 (Z98).